

# A FLEXURAL NORMAL STRESS ANALYSIS IN CABLE-STAYED BRIDGE WITH MULTI-CELLULAR BOX GIRDER CONSIDERING SHEAR LAG PHENOMENON

*By Hiroshi NAKAI\*, Yoneyoshi TAIDO\*\*, Bunji TAKAHASHI\*\*\*  
and Jiro NOGUCHI\*\*\*\**

This paper presents the flexural stress analysis by considering the shear lag phenomenon in the cable-stayed bridges with multi-cellular box girder. For the shear lag phenomenon in the flange plates of such box girders, the parabolic curves with second and fourth orders are assumed, then the corresponding variations of the effective width ratio are investigated and discussed by altering the various shear lag parameters. Based upon these parametric analyses, the additional moment due to shear lag is, moreover simplified to apply the flexural stress analysis of the cable-stayed bridges. Finally, this proposed method is demonstrated by the numerical examples of a cable-stayed bridge with flat multi-cellular box girder.

## 1. INTRODUCTION

In recent years, the long span cable-stayed bridges with multi-cellular flat box girders have been constructed all over the world. For the shear lag analysis of these cable-stayed bridges, there found two distinct researches developed by Nakai · Kotoguchi<sup>1)</sup> and Komatsu · Kitada<sup>2)</sup>. The former is a direct method by using transfer matrix method on the basis of fundamental equation of shear lag derived by references<sup>3)-4)</sup> and the latter proposes an approximate method to evaluate the flexural normal stress due to shear lag without considering the equivalent span length<sup>4)</sup>.

In applying these methods to the analysis of shear lag in a cable-stayed bridge with multi-cellular flat box girder, there are, however, so many unclarified problems how to simplify the complicated calculations such as the determinations of equivalent span length and corresponding stress estimations. This paper, then, aims at a proposition of simple and accurate method for determining the flexural normal stress under the consideration of shear lag phenomenon through various parametric analyses.

First part of this paper presents the variations of effective width due to the assumed patterns of normal stress distributions. For these stress distributions in the flange plates of a box girder, a parabolic curve with 2nd order has been recognized as the appropriate one, hitherto<sup>5)</sup>. According to the study by P. J. Dowling<sup>6)</sup>, it is, nevertheless, more practical to approximate by the parabolic curve with 4th order for a flat box girder. These facts have also been confirmed by model tests<sup>7)</sup> and FSM analyses<sup>8)</sup>. However, it is not yet investigated the differences of effective width of box girder between the assumptions of 2nd and 4th

---

\* Member of JSCE, Dr. Eng., Professor, Dept. of Civ. Eng. Osaka City Univ. (Sumiyoshi-ku, Osaka 558)

\*\* Member of JSCE, Manager, Steel Structural Div. Ishikawajima-Harima Heavy Indst. (Higashi-ku, Osaka 541)

\*\*\* Member of JSCE, Engineer, Planning Div. Hanshin Highway Public Corporation (ditto)

\*\*\*\* Member of JSCE, M. Eng., Consultant Eng., Dept. of Design, Sogo Engineering Inc. (Higashi-yodogawa-ku, Osaka 593)

order parabolic curves, so that this point is detailed in this paper.

Secondly, the property of additional moment,  $m(x)$ , due to shear lag is inquired and an approximate formula is derived through numerical analysis. By applying this formula to the cable-stayed bridges, a simple and practical method for determining their effective width is proposed without using the equivalent span length.

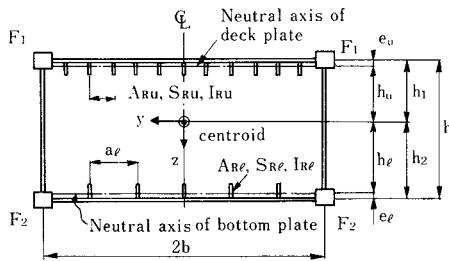
Finally, some numerical calculations concerning prototype of Aji River Bridge<sup>9-10)</sup>, which has four and six multi-cellular box girders and is currently under construction in the highway along Osaka Bay, are shown by combining the method proposed in this paper and the method reported in reference<sup>7)</sup>. Various stress distributions are illustrated and discussed including the negative shear lag phenomenon.

## 2. VARIATIONS OF EFFECTIVE WIDTH DUE TO PATTERNS OF STRESS DISTRIBUTION

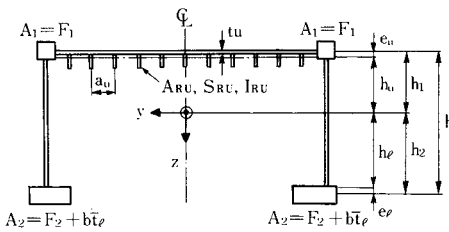
As mentioned in the above, the variations of effective width due to the pterns of the normal stress distribution, i. e. 2nd and 4th order parabolic curves, are inquired by the following analytical study.

### (1) Assumed cross-section

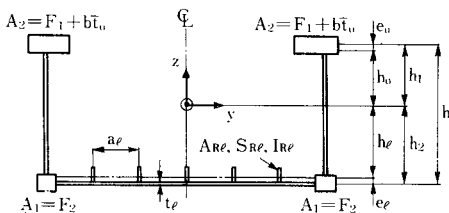
Fig. 1 (a) shows a cross section of ordinary mono-box girder, where the dimensions of top and bottom flange plates are not the same, so that the analysis becomes complicated one. In order to analyze the shear lag of this cross-section as easily as possible without decrease the accuracy, it can be converted into  $\pi$ -shaped girder as shown in Figs. 1 (b) or (c) according to the analytical results in reference 4), in which  $h$ : girder height,  $2b$ : web plate spacing,  $h_1, h_2$ : distance from neutral axis of top or bottom plate to centroid,  $F_1, F_2$ : cross-sectional area of bracket at top or bottom plate,  $a_u, a_l$ : spacing of rib at top or bottom plate,  $A_{Ru}, A_{Rl}$ : cross-sectional area of rib at top or bottom plate,  $S_{Ru}, S_{Rl}$ : geometrical moment of area of rib at top or bottom plate,  $I_{Ru}, I_{Rl}$ : geometrical moment of inertia of rib at top of bottom flange plate.



(a) Original box girder



(b)  $\pi$ -shaped girder with deck Plate



(c)  $\pi$ -shaped girder with bottom plate

Fig. 1 Conversion of Box Girder into  $\pi$ -shaped Girder.

centroid,  $F_1, F_2$ : cross-sectional area of bracket at top or bottom plate,  $a_u, a_l$ : spacing of rib at top or bottom plate,  $A_{Ru}, A_{Rl}$ : cross-sectional area of rib at top or bottom plate,  $S_{Ru}, S_{Rl}$ : geometrical moment of area of rib at top or bottom plate,  $I_{Ru}, I_{Rl}$ : geometrical moment of inertia of rib at top of bottom flange plate.

The parameters  $\alpha, \beta, \omega$  and  $\kappa$  for the shear lag of  $\pi$ -shaped shown in Fig. 2, which is the representative of Figs. 1 (b) and (c), can be summarized in Table 1, where

$t_f (t_u, t_l)$ : thickness of flange plate,  $t_w$ : thickness

Table 1 Parameter  $\alpha, \beta, \omega$  and  $\kappa$ .

Parameters	Parabolic curve with 2nd order <sup>1</sup>	Parabolic curve with 4th order <sup>2</sup>
$\alpha$	$\frac{1}{b} \sqrt{\frac{\beta}{\omega}}$	$\frac{1.195}{b} \sqrt{\frac{\beta}{\omega}}$
$\beta$	$\frac{1.5}{1.2 - \kappa}$	$\frac{1.25}{1.111 - \kappa}$
$\omega$	$\frac{1}{1 - \mu} + \frac{A_r}{at_r} (1 + \mu)$	
$\kappa$	$\frac{A_t + I_t}{A}$	

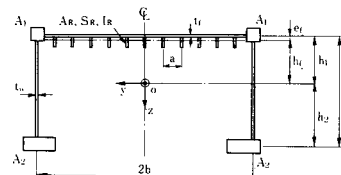
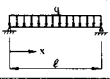
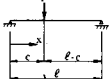


Fig. 2 Cross-section of  $\pi$ -shaped Girder.

Table 2 Solutions of Bending Moment  $M(x)$  and Additional Moment  $m(x)$  due to Shear Lag.

Loading conditions	Parabolic curve with 2nd order <sup>1</sup>	Parabolic curve with 4th order <sup>2</sup>
Uniformly distributed load: $q$ 	$M(x) = \frac{q\ell^2}{2} \left\{ 1 - \left(\frac{x}{\ell}\right)^2 \right\}$ $m(x) = \frac{qb^2\omega}{1 - \frac{\cosh \alpha(x - \frac{\ell}{2})}{\cosh \frac{\alpha\ell}{2}}}$	$m(x) = \frac{0.700qb^2\omega}{1 - \frac{\cosh \alpha(x - \frac{\ell}{2})}{\cosh \frac{\alpha\ell}{2}}}$
Concentrated load: $P$ 	$M(x) = P\ell\left(\frac{x}{\ell}\right) \left\{ 1 - \left(\frac{x}{\ell}\right) \right\}, (0 \leq x \leq c)$ $P\ell\left(\frac{x}{\ell}\right) \left\{ 1 - \left(\frac{x}{\ell}\right) \right\}, (c \leq x \leq \ell)$ $m(x) = \frac{Pb/\omega\beta}{\sinh \alpha \ell} \frac{\sinh \alpha(\ell-c)}{\sinh \alpha c} \sinh \alpha x, (0 \leq x \leq c)$ $\frac{Pb/\omega\beta}{\sinh \alpha \ell} \frac{\sinh \alpha(\ell-x)}{\sinh \alpha c} \sinh \alpha c, (c \leq x \leq \ell)$	$m(x) = \frac{0.837 Pb/\omega\beta}{\sinh \alpha \ell} \frac{\sinh \alpha(\ell-c)}{\sinh \alpha c} \sinh \alpha x, (0 \leq x \leq c)$ $\frac{0.837 Pb/\omega\beta}{\sinh \alpha \ell} \frac{\sinh \alpha(\ell-x)}{\sinh \alpha c} \sinh \alpha c, (c \leq x \leq \ell)$

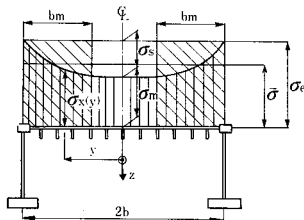


Fig. 3 Normal Stress Distribution and Corresponding Effective Width.

Table 3 Normal Stress and Effective Width Formula for Parabolic Curve with 2nd and 4th Order.

Items	Notations	Parabolic curve with 2nd order <sup>1</sup>	Parabolic curve with 4th order <sup>2</sup>
Normal stress	$\sigma_{x(y)}$ (Stress distribution)	$\sigma_m \cdot \sigma_s \left(\frac{y}{b}\right)^2$	$\sigma_m \cdot \sigma_s \left(\frac{y}{b}\right)^4$
	$\sigma_m$ (Minimum Stress)	$\frac{1}{Wf}  M(x) + (1 - \frac{2}{3}\chi)m(x) $	$\frac{1}{Wf}  M(x) - (1 - \frac{4}{5}\chi)m(x) $
	$\sigma_s$ (Stress Sag)		$\frac{m(x)}{Wf}$
	$\sigma_e$ (Maximum Stress)	$\frac{1}{Wf}  M(x) - \frac{2}{3}\chi m(x) $	$\frac{1}{Wf}  M(x) + \frac{4}{5}\chi m(x) $
	$\bar{\sigma}$ (Elementary beamtheory)		$\frac{M(x)}{Wf}$
Effective width ratio	$\frac{b_m}{b}$	$1 - \frac{\frac{2}{3}m(x)}{M(x) + \frac{2}{3}\chi m(x)}$	$1 - \frac{\frac{4}{5}m(x)}{M(x) + \frac{4}{5}\chi m(x)}$

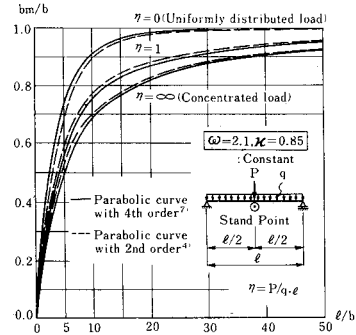


Fig. 4 Comparisons of Effective Width  $b_m/b$  due to Difference of Assumed Stress Distributions.

of web plate,  $a$  ( $a_u, a_l$ ) : spacing of rib,  $A_1, A_2$  : half cross-sectional area of bracket at top or bottom flange plate,  $A_R$  ( $A_{Ru}, A_{Rl}$ ),  $S_R$  ( $S_{Ru}, S_{Rl}$ ),  $I_R$  ( $I_{Ru}, I_{Rl}$ ) : cross-sectional area, geometrical moment of area and geometrical moment of inertia of rib with respect to their neutral axis at top or bottom plate.

$$A_f = b \bar{t}_f = b \left( \frac{t_f}{1 - \mu^2} + \frac{A_R}{a} \right), \quad A_w = t_w h / (1 - \mu^2) \dots \dots \dots (1), (2)$$

$\mu$  : poisson's ratio

$$I_f = 2 A_f h_f^2, \quad I = 2 \{ A_f h_f^2 + (h^2/3 - h_1 h_2) A_w + (b I_R) / a + A_1 h_1^2 + A_2 h_2^2 \} \dots \dots \dots (3), (4)$$

$$A = A_f + A_1 + A_w + A_2, \quad h_1 = \frac{1}{2A} \left\{ (2 A_2 + A_w) h + \frac{2b}{a} S_R \right\} \dots \dots \dots (5), (6)$$

$$h_2 = h - h_1, \quad h_f = h_1 - e_f, \quad e_f = S_R / A_R \dots \dots \dots (7) \sim (9)$$

Bending moment,  $M(x)$ , and additional moment due to the shear lag,  $m(x)$ , can also be given in Table 2. The formulae for estimating the normal stress,  $\sigma_x(y)$ , at an arbitrary point shown in Fig. 3 and the effective width,  $b_m$ , can be listed in Table 3, where

$$W_f = \frac{(1 - \mu^2) I}{h_f} \dots \dots \dots (10)$$

(2) Variations of effective width due to load intensity ratio

Fig. 4 and Table 4 show the variations of the effective width ratio,  $b_m/b$ , due to the load intensity ratio,  $\eta$ , given by;

$$\eta = P / (q l) \dots \dots \dots (11)$$

in which  $P$  : intensity of concentrated load,

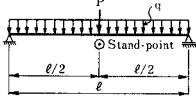
$q$  : intensity of uniformly distributed load,

$l$  : span length of simple beam.

Observing these figure and table, it seems that  $b_m/b$  for 4th order is smaller than one for 2nd order

Table 4 Variations of Effective Width Ratio  $b_m/b$  due to Difference of Assumed Stress Distribution.

Parameters	$\eta=0$			$\eta=0.2$			$\eta=0.5$			$\eta=1.0$			$\eta=\infty$		
	2nd	4th	$\epsilon(\%)$	2nd	4th	$\epsilon(\%)$	2nd	4th	$\epsilon(\%)$	2nd	4th	$\epsilon(\%)$	2nd	4th	$\epsilon(\%)$
5	0.676	0.715	5.8	0.633	0.644	1.7	0.603	0.597	-1.0	0.582	0.564	-3.1	0.524	0.507	-3.2
10	0.898	0.913	1.7	0.839	0.837	-0.2	0.799	0.787	-1.5	0.769	0.752	-2.2	0.701	0.688	-1.9
20	0.973	0.977	0.4	0.931	0.927	-0.4	0.901	0.893	-0.9	0.880	0.867	-1.5	0.829	0.820	-1.1
30	0.988	0.990	0.2	0.957	0.954	-0.3	0.935	0.929	-0.6	0.919	0.910	-1.0	0.880	0.874	-0.7
40	0.993	0.994	0.1	0.969	0.966	-0.3	0.952	0.947	-0.5	0.939	0.931	-0.9	0.908	0.903	-0.6
50	0.996	0.996	0.0	0.976	0.974	-0.2	0.962	0.957	-0.5	0.951	0.945	-0.6	0.925	0.921	-0.4



Parameters

$$\eta = \frac{P}{q \cdot l}$$

$$\omega = 2.1$$

$$\chi = 0.85 \text{ Constant}$$

$$\epsilon = \frac{4th - 2nd}{2nd} \times 100 (\%)$$

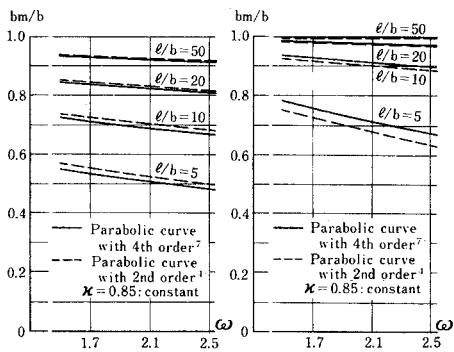
when parameter becomes large, whereas  $b_m/b$  for 2nd order is smaller than 4th order in accordance with the decrease of  $\eta$ . Namely, if the stress distribution is assumed as the parabolic curve with 4th order, the value of effective ratio becomes larger than 2nd order near the mid-span where the influence of  $q$  is superior and smaller than 2nd order at the section where  $P$  is predominant.

(3) Variations of effective width due to parameters  $\omega$  and  $\chi$

The variations of effective width at mid-span due to parameters  $\omega$ , which represents the statical properties of flange plates, can be plotted in Fig. 5. It can be seen from this figure that the influence of parameter  $\omega$  has the similar tendency to both 2nd and 4th orders. While, Fig. 6 shows the variations of  $b_m/b$  at mid-span due to the parameter  $\chi$  which predicts the cross-sectional property of box girder. From this figure, there recognizes the tendency to increase  $b_m/b$  in accordance with the increase of  $\chi$  for the uniformly distributed load and the differences between 2nd and 4th order are small. For a concentrated load,  $b_m/b$  decreases with increase of  $\chi$  and the variation of 4th order is somewhat larger than 2nd order.

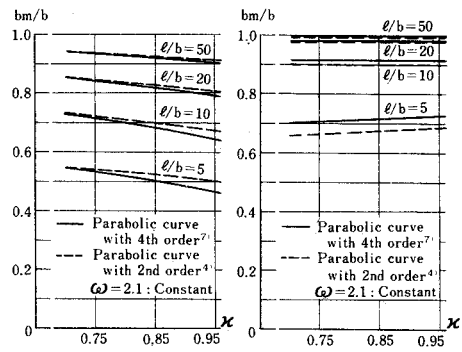
According to the design code of BS 5400 part 3<sup>12)</sup>, the normal stress distribution of box girder is assumed as 4th order parabolic curve and the effective width ratio is given by the tables for a simple beam with the uniformly distributed load and for a continuous beam with a concentrated load  $P$  (reaction) at an intermediate support of continuous beam. The comparisons between the results obtained by this paper and those of BS 5400 part 3<sup>12)</sup> are illustrated in Fig. 7. It seems that the quite well agreements can be recognized between them and the validity of the analytical method predicated in this paper can be confirmed through these numerical calculations.

Consequently, it is concluded that the differences of effective width ratio due to two assumptions are not so large except the region where  $l/b$  is small, but one may be estimated the effective width on the basis of



(a) Concentrated load (b) Uniformly distributed load

Fig. 5 Variations of Effective Width  $b_m/b$  due to Parameter  $\omega$  (midspan of simply supported girder).



(a) Concentrated load (b) Uniformly distributed load

Fig. 6 Variations of Effective Width  $b_m/b$  due to Parameter  $\chi$  (midspan of simply supported girder).

the assumptions either of 2nd or 4th order parabolic curves.

### 3. SIMPLIFICATION OF ADDITIONAL MOMENT

The moment diagram of a cable-stayed bridge represents the complex distributions, because the main girder is supported by not only intermediate supports but also many cables. Therefore, it is difficult to fix the equivalent span by finding two points where the bending moments are equal to zero. To avoid such a complicated procedure and errors included in the calculations of effective width, let us consider an approximate but accurate method for determining the effective width of cable-stayed bridges without introducing the equivalent span length.

In general, the effective width can easily be determined from the fundamental equation, shown in Table 3, provided that bending moment,  $M(x)$ , and additional moment,  $m(x)$ , are known. If the distributions of  $m(x)$  are investigated numerically, then corresponding effective width formula can be much more simplified.

Now, it is assumed in the preceding discussions that the normal stress of a flat box girder is distributed as 4th order parabolic curve. The corresponding distributions of additional moment,  $m(x)$ , in Table 2 can be plotted as shown in Fig. 8, which can also be simplified as follows;

#### (1) Uniformly distributed load

When the variable  $\alpha l$  of hyperbolic function is large enough, the value  $e^{-\alpha l}$  can be set as  $e^{-\alpha l} \cong 0$ . Thus, the additional moment  $m(x)$  can be set by;

$$m(x) = 0.700 qb^2 \omega \left\{ 1 - \frac{\cosh \alpha(x-l/2)}{\cosh(\alpha l)/2} \right\}$$

$$\cong 0.700 qb^2 \omega (1 - e^{-\alpha x} - e^{-\alpha x'})$$

where  $x'$  denotes the distance from the right end support to a considering point as shown in Fig. 8. Moreover, the parameter  $\alpha$  is usually greater than  $1.5/b$ , so that  $e^{-\alpha x} \cong 0$  at  $x \geq 2b$  and  $e^{-\alpha x'} \cong 0$  at  $x' \geq 2b$ , where  $2b$  is the girder width. Since the errors induced to the effective width by these approximations is less than a few percentages, thus  $m(x)$  can be expressed as follows;

$$m(x) = 0.700 qb^2 \omega \dots \dots \dots (12)$$

#### (2) Concentrated load

In the similar manner to the above,  $m(x)$  can be simplified as follows;

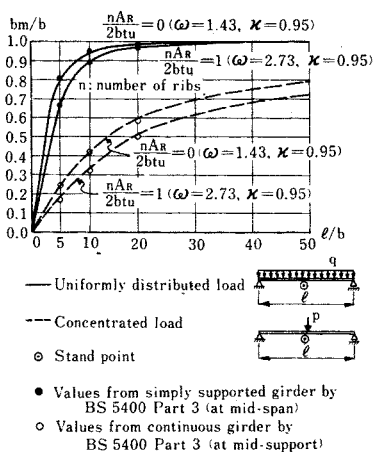


Fig. 7 Comparisons of Effective Width Ratio  $d_m/b$  between Proposed Method and BS 5400 Part 3.

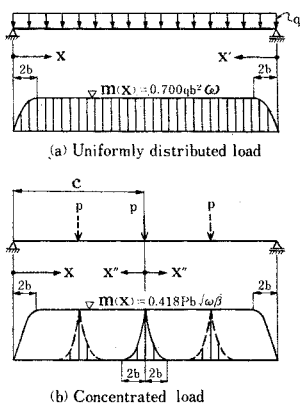


Fig. 8 Distribution of Additional Moment  $m(x)$  in Direction of Span.

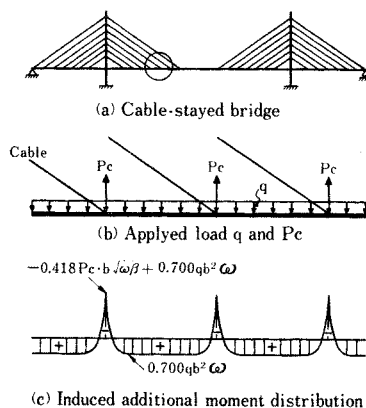


Fig. 9 Additional Moment Distribution  $m(x)$  in Cable-Stayed Bridge.

$$m(x) = 0.837 P b \sqrt{\omega \beta} \frac{\sinh \alpha(l-c)}{\sinh \alpha l} \sinh \alpha x$$

$$\cong 0.418 P b \sqrt{\omega \beta} \cdot e^{-\alpha x}$$

where  $x''$  is the distance from loading point to considering point (see Fig. 8). The maximum additional moment occurs at the loading point,  $x''=0$ , then the above equation can be written as ;

$$m(x) = 0.418 P b \sqrt{\omega \beta} \dots \dots \dots (13)$$

If the intensities of applied uniformly distributed load  $q$  and concentrated load  $P$  as well as the reactions  $R_c$  due to cables and intermediate supports are known, the additional moment can easily be obtained by superposing Eqs. (12) and (13). For example, the distributions of  $m(x)$  near the cable supported portion of a cable-stayed bridge can be illustrated in Fig. 9. In this case, the region, where the additional moment  $m(x)$  due to a concentrated load should be taken, is less than  $2b$  (girder width) from a considering point by judging from the following equation.

$$m(x)/|m(x)|_{\max} = e^{-\alpha x} \dots \dots \dots (14)$$

#### 4. APPLICATIONS TO FLEXURAL STRESS ANALYSIS OF CABLE-STAYED BRIDGE

Let us show the numerical examples and discuss the flexural stress due to shear lag of a cable-stayed bridge with the flat multi-cellular box girder by using the preliminary design data of Aji Rive Rridge<sup>(9)-10)</sup>. This cable-stayed bridge is a multiple and fun type as shown in Fig. 10. The cross-section is detailed in Fig. 11 and their dimensions are summarized in Table 5.

By adopting the results of additional moment  $m(x)$  derived by this paper and the method for evaluating the flexural stress in flat multi-cellular box girder proposed in reference 7), the various numerical calculations are carried out as follows ;

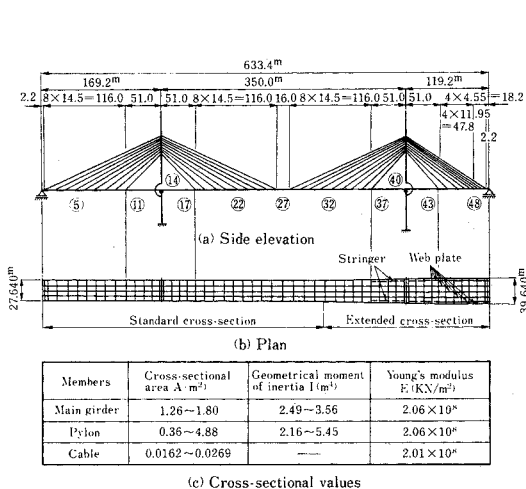


Fig. 10 Analytical Model of Aji River Bridge.

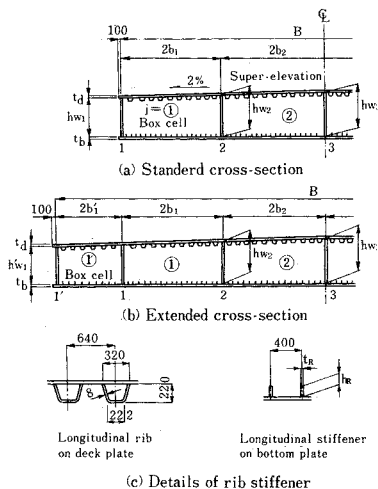


Fig. 11 General Cross-Section of Main Girder in Aji River Bridge.

Table 5 Cross-sectional Dimensions of Main Girder in Aji River Bridge.

View points	Box girder width (m)				Box girder depth (m)				Plate element thickness (mm)			Longitudinal stiffener (mm)	
	2b <sub>1</sub>	2b <sub>2</sub>	2b <sub>1</sub> '	B	hw <sub>1</sub>	hw <sub>2</sub>	hw <sub>1</sub>	hw <sub>1</sub>	td	tb	tw	ha	ta
5	6.72	7.10		27.64	2.92	3.06	3.20		12	12	12	190	15
11	6.72	7.10		27.64	2.92	3.06	3.20		12	12	12	190	15
16	6.72	7.10		27.64	2.92	3.06	3.20		12	15	14	210	19
17	6.72	7.10		27.64	2.92	3.06	3.20		12	12	12	190	15
22	6.72	7.10		27.64	2.92	3.06	3.20		12	12	12	190	15
27	6.72	7.10		27.64	2.92	3.06	3.20		12	12	12	190	15
32	7.20	7.10		28.60	2.91	3.06	3.20		12	12	12	190	15
37	10.05	7.10		34.30	2.86	3.06	3.20		12	12	12	190	15
43	11.42	7.10		37.03	2.83	3.06	3.20		12	18	16	230	22
48	12.30	7.10		38.80	2.81	3.06	3.20		12	12	12	190	15
53	8.35	7.10	4.37	39.64	2.89	3.06	3.20	2.80	12	14	12	190	15

(1) Procedures of analysis

a) The cable-stayed bridge, shown in Fig. 10, is analyzed by regarding the main girder as a single plane structure. For evaluating the flexural rigidity of main girder, the cross-section is perfectly effective without considering the effective width as pointed out by reference 7). The intensities of concentrated load  $P$  (live load and reactions due to cables and intermediate supports) and uniformly distributed load  $q$  (dead and live loads) as well as the maximum or minimum values of bending moment,  $M(x)$ , at the considering points are stored in the computer memories.

b) Next, the additional moments,  $m(x)$ , are calculated for each flat box girder by using the above  $P$  and  $q$ . The corresponding effective width ratio,  $b_{mj}/b_j$ , can be obtained by using  $m(x)$ ,  $M(x)$  and the formula given in Table 3.

c) The multi-cellular flat box girder is, then, idealized into a multiple I-girder according to the method described in reference 7). Thus, the applied bending moment  $M_i(x)$  for each I-girder can be estimated proportional to their flexural rigidity. The flexural normal stress can also be evaluated on the basis of the above effective width ratio  $b_{mj}/b_j$ .

d) Finally, the stress enlargement coefficient for the outer side of I-girders must be determined so as to model the secondary shear lag throughout the multi-cellular flat box girder<sup>7)</sup>. In this analysis alone, the equivalent span, which is the distance between two points where the corresponding bending moments  $M(x)$  are equal to zero, is required. The equivalent span for Aji River Bridge can be drawn in Fig. 12.

(2) Effective width for each box cells

The cross-section of Aji River Bridge is significantly wide and the top and bottom flange plates have so many ribs as is seen from Fig. 11 and Table 5, that the parameters  $\omega$  and  $\kappa$  have almost constant values within the ranges  $\omega=2.2\sim 2.4$  and  $\kappa=0.93\sim 0.95$ .

Besides, since the parameter  $\alpha$  almost equals to  $2.0/b$ , the effects of concentrated loads apart from the considering point may practically be ignored.

According to the above two reasons, the effective width ratio for each cells can approximately evaluated from  $m(x)$  in Eqs. (12) and (13) as well as the general equation of Table 3 as follows ;

$$\frac{b_{mj}}{b_j} = \left(1 - \frac{4\lambda}{5 + 3.8\lambda}\right) \dots\dots\dots (15)$$

where  $b_{mj}$  : effective width ratio each box cell,  $b_j$  : half of web plate spacing for each box cell,  
 $\lambda = m(x)/M(x)$ ..... (16)

For the case  $\lambda \leq 0$  in the above equation, there occurs the negative shear lag<sup>11)</sup> as explained latter, one should be put  $\lambda=0$  from the conservative point of view, and

$$m(x) = 1.7 P b_j + 1.6 q b_j^2 \dots\dots\dots (17)$$

in which the coefficients 1.7 and 1.6 correspond to the parameters  $\omega=2.3$  and  $\kappa=0.94$ .

Note that the applied load  $P$  and  $q$  must be taken as the intensity throughout the girder.

(3) Numerical examples of effective width

Table 6 shows the calculated results of effective width ratio  $b_{mj}/b_j$  for 11 considering points indicated in Fig. 10, in which the points signed with the symbol \* are ones where the negative shear lag takes place. The stress distribution in the flange plate for such cases can be illustrated in Fig. 13. However, the bending moments for these sections are generally so small, that one can practically be treated by considering the whole section as effective. For the sake of convenience,  $b_{mj}/b_j$  can, therefore, be put as 1.0 for these section as shown in Table 6.

Fig. 14 shows the variations of effective width ratio  $b_{m2}/b_2$  at inner box cell  $j=2$  in the direction of span for various loading conditions. Observing this figure, it is obvious that the effective width becomes

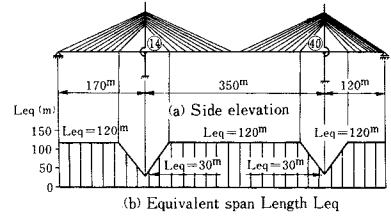


Fig. 12 Equivalent Span Length  $L_{eq}$  for Stress Enlargement Coefficient  $\rho$ .

Table 6 Effective Width Ratio  $b_m/b_j$  for each Box Cell.

Loading condition	point	M (kN.m)	P (kN)	q (kN/m)	Box cell ①		Box cell ②		Box cell ③	
					m (kN.m)	bm 1/b 1	m (kN.m)	bm 2/b 2	m (kN.m)	bm 1/b 1
Dead load and Prestress	5	872	-3653	264	-16100	1.000	-16720	1.000		
	11	64120	0	254	4588	0.946	5122	0.940		
	14	-82590	-18060	296	-97810	0.501	-103000	0.488		
	17	57390	0	250	4516	0.940	5041	0.934		
	22	11350	-3887	265	-17420	0.433	-18120	0.423		
	27	-6056	0	265	4787	1.000	5343	1.000		
	32	14320	-3834	269	-17890	1.000	-17710	1.000		
	37	82990	0	310	12520	0.892	6251	0.943		
	40	142300	-24470	380	-217700	0.434	-140000	0.550		
	43	51860	0	329	19910	0.762	6634	0.907		
48	94630	-4233	391	-19140	0.860	-17660	0.869	-12737	0.902	
Live load (max.)	5	78950	957	52	6406	0.939	6824	0.935		
	11	34470	1217	52	7891	0.844	8393	0.836		
	14	4351	467	0	2668	0.665	2818	0.653		
	17	34250	1217	52	7891	0.843	8393	0.835		
	22	48950	516	52	3887	0.940	4163	0.936		
	27	50470	1217	52	7891	0.888	8393	0.882		
	32	49090	542	53	4416	0.933	4340	0.934		
	37	41540	1397	63	14480	0.780	9701	0.841		
	40	7977	1079	0	10470	0.474	6512	0.597		
	43	58090	1517	70	20100	0.781	10570	0.872		
48	70690	1648	71	13680	0.864	11380	0.884	6664	0.929	
Live load (min.)	5	-5788	-513	0	-2930	0.961	3096	0.959		
	11	-2380	0	0	1000	0	1000	0		
	14	55570	5318	52	-29440	0.698	-31050	0.686		
	17	-25170	0	0	1000	0	1000	0		
	22	29060	-272	0	-1554	0.959	-1642	0.957		
	27	10450	0	0	1000	0	1000	0		
	32	-29630	-293	0	-1793	0.954	-1768	0.954		
	37	-30700	0	0	1000	0	1000	0		
	40	-75420	-7380	67	-68140	0.571	-43190	0.681		
	43	40160	0	0	1000	0	1000	0		
48	71890	-1024	0	-7268	0.925	-6180	0.935	-3804	0.959	

Note ✕ Shows negative shear lag

Table 7 Normal Stress  $\sigma$  at Upper Flange for each Idealized I-Girder.

Point	Idealized I-Girder i=	Dead load and prestress (D+P.S.)									Live load (max.)									Live load (min.)								
		$\sigma$			$\bar{\sigma}$			$\sigma/\bar{\sigma}$			$\sigma$			$\bar{\sigma}$			$\sigma/\bar{\sigma}$			$\sigma$			$\bar{\sigma}$			$\sigma/\bar{\sigma}$		
		$\sigma$	$\bar{\sigma}$	$\sigma/\bar{\sigma}$	$\sigma$	$\bar{\sigma}$	$\sigma/\bar{\sigma}$	$\sigma$	$\bar{\sigma}$	$\sigma/\bar{\sigma}$	$\sigma$	$\bar{\sigma}$	$\sigma/\bar{\sigma}$	$\sigma$	$\bar{\sigma}$	$\sigma/\bar{\sigma}$	$\sigma$	$\bar{\sigma}$	$\sigma/\bar{\sigma}$	$\sigma$	$\bar{\sigma}$	$\sigma/\bar{\sigma}$	$\sigma$	$\bar{\sigma}$	$\sigma/\bar{\sigma}$			
⑤	1	-0.5	-0.5	1.00	-48.6	-44.0	1.10	34.9	32.2	1.08																		
	2	-0.5	-0.5	1.00	-48.9	-46.0	1.06	35.0	33.7	1.04																		
	3	-0.6	-0.6	1.00	-51.3	-48.0	1.07	36.7	35.2	1.04																		
⑪	1	-40.0	-35.8	1.12	-23.8	-19.2	1.24	13.7	12.8	1.07																		
	2	-39.5	-37.3	1.06	-23.7	-20.1	1.18	13.4	13.4	1.00																		
	3	-41.5	-39.0	1.06	-24.9	-21.0	1.19	14.0	14.0	1.00																		
⑭	1	89.2	44.6	2.00	-3.7	-2.4	1.54	46.0	30.0	1.53																		
	2	90.1	47.1	1.91	-3.6	-2.5	1.44	44.7	31.8	1.41																		
	3	95.2	49.2	1.93	-3.8	-2.5	1.52	47.0	33.1	1.42																		
⑰	1	-35.8	-31.8	1.13	-23.6	-19.1	1.24	15.0	14.0	1.07																		
	2	-35.4	-33.2	1.07	-23.6	-20.0	1.18	14.7	14.7	1.00																		
	3	-37.0	-34.7	1.07	-24.8	-20.9	1.19	15.3	15.3	1.00																		
⑳	1	13.4	6.4	2.09	-30.0	-27.2	1.10	17.5	16.2	1.08																		
	2	14.8	6.6	2.21	-30.3	-28.5	1.06	17.6	17.0	1.04																		
	3	15.4	6.9	2.23	-31.8	-29.8	1.07	18.4	17.7	1.04																		
㉑	1	3.5	3.3	1.06	-32.6	-28.1	1.16	6.1	5.8	1.05																		
	2	3.5	3.5	1.00	-33.0	-29.4	1.12	6.1	6.1	1.00																		
	3	3.7	3.7	1.00	-34.6	-30.8	1.12	6.4	6.4	1.00																		

Table 8 Normal Stress  $\sigma$  at Lower Flange for each Idealized I-Girder.

Point	Idealized I-Girder i=	Dead load and prestress (D+P.S.)									Live load (max.)									Live load (min.)								
		$\sigma$			$\bar{\sigma}$			$\sigma/\bar{\sigma}$			$\sigma$			$\bar{\sigma}$			$\sigma/\bar{\sigma}$			$\sigma$			$\bar{\sigma}$			$\sigma/\bar{\sigma}$		
		$\sigma$	$\bar{\sigma}$	$\sigma/\bar{\sigma}$	$\sigma$	$\bar{\sigma}$	$\sigma/\bar{\sigma}$	$\sigma$	$\bar{\sigma}$	$\sigma/\bar{\sigma}$	$\sigma$	$\bar{\sigma}$	$\sigma/\bar{\sigma}$	$\sigma$	$\bar{\sigma}$	$\sigma/\bar{\sigma}$	$\sigma$	$\bar{\sigma}$	$\sigma/\bar{\sigma}$	$\sigma$	$\bar{\sigma}$	$\sigma/\bar{\sigma}$	$\sigma$	$\bar{\sigma}$	$\sigma/\bar{\sigma}$			
⑤	1	0.5	0.5	1.00	50.4	45.7	1.10	-36.2	-33.4	1.08																		
	2	0.5	0.5	1.00	51.0	47.9	1.06	-36.6	-35.1	1.04																		
	3	0.6	0.5	1.00	53.4	50.2	1.06	-38.2	-36.8	1.04																		
⑪	1	41.5	37.0	1.12	24.6	19.9	1.24	-14.2	-13.3	1.07																		
	2	41.2	38.9	1.06	24.7	21.0	1.18	-14.0	-14.0	1.00																		
	3	43.2	40.7	1.06	26.0	21.9	1.19	-14.7	-14.7	1.00																		
⑭	1	-77.8	-37.9	2.05	3.2	2.0	1.60	-39.6	-25.5	1.55																		
	2	-76.7	-39.3	1.95	3.0	2.1	1.43	-37.6	-26.5	1.42																		
	3	-81.1	-41.2	1.97	3.2	2.2	1.45	-39.7	-27.6	1.44																		
⑰	1	-37.1	-33.0	1.12	24.5	19.8	1.24	-15.5	-14.6	1.06																		
	2	-36.8	-34.6	1.06	24.6	20.8	1.18	-15.3	-15.3	1.00																		
	3	-43.2	-40.7	1.06	26.0	21.9	1.19	-14.7	-14.7	1.00																		
⑳	1	-13.8	-6.6	2.10	31.3	28.3	1.10	-18.2	-16.8	1.08																		
	2	-15.2	-6.9	2.20	31.6	29.7	1.06	-18.4	-17.6	1.05																		
	3	-16.0	-7.3	2.19	33.1	31.1	1.06	-19.2	-18.4	1.04																		
㉑	1	-3.6	-3.5	1.03	33.8	29.2	1.16	-6.3	-6.1	1.03																		
	2	-3.7	-3.7	1.00	34.4	30.7	1.12	-6.4	-6.4	1.00																		
	3	-3.8	-3.8	1.00	36.1	32.0	1.13	-6.7	-6.7	1.00																		

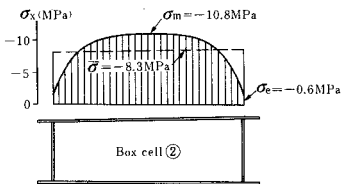


Fig. 13 Stress Distribution  $\sigma_x(y)$  due to Negative Shear Lag at Point ⑰ under Dead Load.

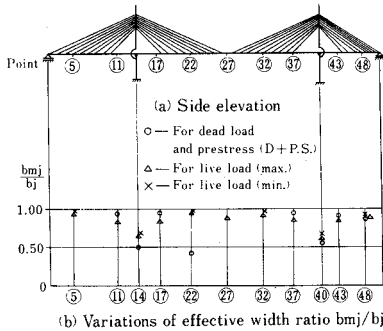


Fig. 14 Variations of Effective width Ratio in Direction of Span.

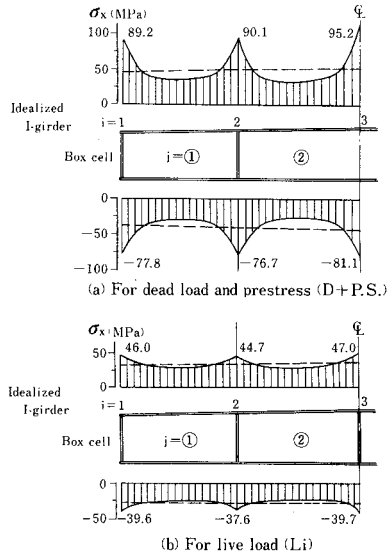


Fig. 15 Distributions of Normal stress  $\sigma_x(y)$  (point ⑪).



remarkably small where the concentrated load is predominant. The effective width for dead load at the section ㉓ becomes small, but the shear lag phenomenon does not govern the proportioning of cross-section, since the bending moment is small. The effective width at cross-section ㉔ is also small and this may be caused by the effects of concentrated load due to cable with sharp angle.

#### (4) Normal stress distribution

The normal stress distributions can be summarized as shown in Table 7 and 8 by adopting the effective width in Fig. 12 and stress enlargement factor  $\rho$  in Eqs. (26) and (27) in reference 7). The stress distributions for typical cross-section ㉔ can also be plotted in Fig. 15. From this figure, the stress at the junction point of exterior web and flange plates is not greater than the other points in spite of the consideration of stress enlargement factor  $\rho$ . This is caused by the reduction of girder height by super elevation of top plate (2%) and the distributed bending moment, of which value is proportional to the flexural rigidity, becomes somewhat small.

It should be noted that the stress enlargement factor  $\rho$  at the expanded part with 6 box cells is different from the values reported in reference 7). Then, this factor  $\rho$  has been determined by FEM analysis at the similar manner to reference 7), but their details are omitted herein.

## 5. CONCLUSION

This paper proposed a method for estimating the flexural normal stress in a cable-stayed bridge with the flat multi-cellular box girders by considering shear lag phenomenon. The main conclusions can be summarized as follows;

(1) This difference between effective width ratio is practically small even in the case where the normal stress distributions are assumed as either 2nd or 4th order parabolic curves.

(2) Thus, the variations of additional moment due to shear lag are investigated on the assumption of 4th order parabolic normal stress distribution on the flange plates. Then, a simple and practical method to evaluate the effective width is developed without considering the equivalent span length.

(3) The numerical method to calculate the flexural normal stress in the cable-stayed bridge with a flat multi-cellular box girder is detailed together with the numerical examples by combining the method developed in reference 7).

(4) Through these analyses, it is shown that this method can practically be applied to continuous bridges, cable-stayed bridges and so on.

## 6. ACKNOWLEDGMENTS

In writing this paper, the authors are indebted to all the members of Technical Committee on Highway along Osaka Bay, Hanshin Expressway Public Corporation, for their valuable advices and suggestion. Our thanks are also due to; Mr. S. Fukuoka and Mr. H. Hayashi of Hanshin Expressway Public Corporation in conducting the numerical calculations.

## REFERENCES

- 1) Nakai, H. and Kotoguchi, H. : Analysis of Effective Width for Continuous Steel Girder Bridges by Transfer Matrix Method, Proc. of JSCE, No. 251, July, 1976.
- 2) Komatsu, S. and Kitada, T. : Shear Lag Analysis of Cable Stayed Girder Bridges and its Application to Design Calculation, Proc. of JSCE, No. 254, Oct. 1976.
- 3) Komatsu, S. : On Shear Lag in Continuous Box Girder, Trans. of JSCE, No. 58, Sept. 1958.
- 4) Kondo, K., Komatsu, S. and Nakai, H. : Theoretical and Experimental Researches on Effective Width of Girder Bridges with Steel Deck Plates, Trans. of JSCE, No. 86, Oct. 1962.
- 5) Reissner, E. : Analysis of Shear Lag in Box Beam by Principal of Minimum Potential Energy, Quarterly of Applied Mathematics, Vol. 4, No. 3, 1946.
- 6) Moffatt, K.R. and Dowling P.J. : Shear Lag in steel box girder bridges, The Structural Engineer, No. 10, Vol. 53, Oct. 1975.

- 7) Nakai, H., Taido, Y. and Hayashi, H. : An Analysis of Shear Lag and Calculation of Effective Width of Flat Box Girder with Multicells, Proc. of JSCE, No. 340, Dec. 1983.
- 8) Nakai, H., Taido, Y. and Ohta, S. : Analytical and Experimental Studies on Shear Lag in Multi-Cellular Box Girders, Memoirs of Faculty of Engineering, Osaka City University, Vol. 24, Dec. 1983.
- 9) Taido, Y., Fukumoto, S. and Hayashi, H. : Design of a Long span Cable-Stayed Bridge-Aji River Bridge, Jour. of JSCE, Vol. 69, June 1984.
- 10) Takemoto, A., Taido, Y. and Emi, S. : Structure of Aji River Cable-Stay Bridge, Bridge and Foundation Engineering, Vol. 14, March 1980.
- 11) Nakai, H. and Murayama, Y. : Researches on Negative Shear Lag of Cantilever Beams and Application to Bridge Design, Proc. of JSCE, No. 256, Dec. 1976.
- 12) British Standard Institution : BS 5400 Part 3, Code of practice for design of steel bridges, April 1982.

(Received September 17 1984)

---